

AD-A164 502

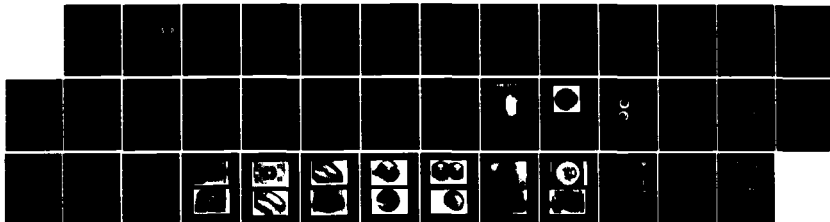
IMPLEMENTATION OF AN IONOSPHERIC-IMAGE FILE MANAGEMENT
PROCESSING AND DIS. (U) PHYSICAL DYNAMICS INC BELLEVUE
WA R D LUCAS ET AL. 15 APR 85 PD-MN-85-331R
AFGL-TR-85-0082 F19628-84-C-0131

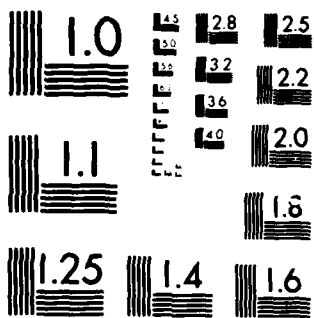
1/1

UNCLASSIFIED

F/8 4/1

NL





MICROCOPY RESOLUTION TEST CHART
NATIONAL BUREAU OF STANDARDS 1963-A

12

AFGL-TR-85-0082

PHASE I FINAL REPORT: IMPLEMENTATION OF AN
IONOSPHERIC-IMAGE FILE MANAGEMENT, PROCESSING,
AND DISPLAY SYSTEM

R. David Lucas
Robert E. Robins

Physical Dynamics, Inc.
300 120th Ave. NE
Bellevue, WA 98009

DTIC
ELECTE
FEB 21 1986
S D D

AD-A164 502

Final Report
~~September 1984 - March 1985~~
1 Sept. 1981 - 28 Feb 1985

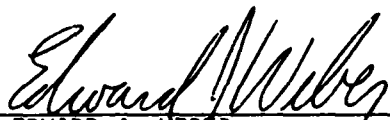
15 April 1985

Approved for public release; distribution unlimited

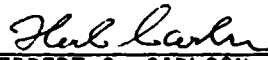
AIR FORCE GEOPHYSICS LABORATORY
AIR FORCE SYSTEMS COMMAND
UNITED STATES AIR FORCE
HANSCOM AFB, MASSACHUSETTS 01731

PHYSICAL DYNAMICS, INC.

"This technical report has been reviewed and is approved for publication"

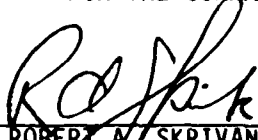


EDWARD J. WEBER
Contract Manager
Ionospheric Effects Branch



HERBERT C. CARLSON, Chief
Ionospheric Effects Branch
Ionospheric Physics Division

FOR THE COMMANDER



ROBERT A. SKRIVANEK
Director
Ionospheric Physics Division

This report has been reviewed by the ESD Public Affairs Office (PA) and is releasable to the National Technical Information Service (NTIS).

Qualified requestors may obtain additional copies from the Defense Technical Information Center. All others should apply to the National Technical Information Service.

If your address has changed, or if you wish to be removed from the mailing list, or if the addressee is no longer employed by your organization, please notify AFGL/DAA, Hanscom AFB, MA 01731. This will assist us in maintaining a current mailing list.

AFGL-TR-85-0096

STUDY OF LARGE AEROSOL PARTICLES

D. J. HOFMANN
J. M. ROSEN

University of Wyoming
Department of Physics & Astronomy
Laramie, Wyoming 82071

Final Report

ERRATA

Period Covered in Block 13b of the DD Form 1473 should read as follows and not as shown:

1 December 1981 - 28 February 1985

AIR FORCE GEOPHYSICS LABORATORY
AIR FORCE SYSTEMS COMMAND
UNITED STATES AIR FORCE
HANSCOM AIR FORCE BASE, MASSACHUSETTS 01731

UNCLASSIFIED

SECURITY CLASSIFICATION OF THIS PAGE

REPORT DOCUMENTATION PAGE

1a. REPORT SECURITY CLASSIFICATION UNCLASSIFIED		1b. RESTRICTIVE MARKINGS NONE	
2a. SECURITY CLASSIFICATION AUTHORITY		3. DISTRIBUTION/AVAILABILITY OF REPORT Approved for public release; distribution unlimited	
2b. DECLASSIFICATION/DOWNGRADING SCHEDULE			
4. PERFORMING ORGANIZATION REPORT NUMBER(S) PD-NW-85-331R		5. MONITORING ORGANIZATION REPORT NUMBER(S) AFGL-TR-85-0082	
6a. NAME OF PERFORMING ORGANIZATION Physical Dynamics, Inc.	6b. OFFICE SYMBOL (If applicable)	7a. NAME OF MONITORING ORGANIZATION Air Force Geophysics Laboratory	
6c. ADDRESS (City, State and ZIP Code) 300 120th Ave NE, Bldg. 7, Suite 220 P.O. Box 3027 Bellevue, WA 98009		7b. ADDRESS (City, State and ZIP Code) Hanscom AFB, MA 01731	
8a. NAME OF FUNDING/SPONSORING ORGANIZATION Electronic Systems Division	8b. OFFICE SYMBOL (If applicable) FQ7620	9. PROCUREMENT INSTRUMENT IDENTIFICATION NUMBER F19628-84-C-0131	
8c. ADDRESS (City, State and ZIP Code) Air Force Systems Command, USAF Hanscom AFB, MA 01731		10. SOURCE OF FUNDING NOS.	
		PROGRAM ELEMENT NO. 65502F	PROJECT NO. 5502
		TASK NO. 01	WORK UNIT NO. AA
11. TITLE (Include Security Classification) PHASE I FINAL REPORT: (U)			
12. PERSONAL AUTHOR(S) R. David Lucas and Robert E. Robins			
13a. TYPE OF REPORT Final	13b. TIME COVERED FROM SEP 84 TO MAR 85	14. DATE OF REPORT (Yr., Mo., Day) April 15, 1985	15. PAGE COUNT 36
16. SUPPLEMENTARY NOTATION <i>Dec. 1981 - 28 Feb. 1985</i>			
17. COSATI CODES		18. SUBJECT TERMS (Continue on reverse if necessary and identify by block number)	
FIELD	GROUP	SUB. GR.	
		image processing, ionosphere, All-Sky camera, aurora	
19. ABSTRACT (Continue on reverse if necessary and identify by block number)			
<p>This Phase I SBIR project addressed the problem of processing the All-Sky Imaging Photometer (ASIP) images collected in support of ionospheric science programs at AFGL and elsewhere. Hardware and software tools are developed that efficiently transform any image of interest to suitable world coordinates, thus removing the geometric distortions introduced by the ASIP wide-angle lens. Interactive graphical tools are demonstrated for the composite display of multiple, concurrent ASIP images, in geometrically corrected form, with a variety of correlative data from other sensor systems. Such systems might include incoherent-scatter radar, the HILAT satellite, and others.</p> <p>Eighteen color plates are presented showing examples of actual ASIP images and test patterns in both raw and geometrically corrected form. Results demonstrating the resolution requirements of the ASIP data are included. Various aspects of the geometrical transformation and image-enhancement processing are illustrated, and example composite displays with actual ASIP and HILAT data are presented. (Continued on next page.)</p>			
20. DISTRIBUTION/AVAILABILITY OF ABSTRACT UNCLASSIFIED/UNLIMITED <input type="checkbox"/> SAME AS RPT. <input type="checkbox"/> DTIC USERS <input type="checkbox"/>		21. ABSTRACT SECURITY CLASSIFICATION UNCLASSIFIED	
22a. NAME OF RESPONSIBLE INDIVIDUAL Edward J. Weber		22b. TELEPHONE NUMBER (Include Area Code) (617) 861-4192	22c. OFFICE SYMBOL LIS

DD FORM 1473, 83 APR

EDITION OF 1 JAN 73 IS OBSOLETE.

SECURITY CLASSIFICATION OF THIS PAGE

11. TITLE

IMPLEMENTATION OF AN IONOSPHERIC-IMAGE FILE MANAGEMENT, PROCESSING, AND DISPLAY SYSTEM

19. ABSTRACT (continued)

- Phase I focused on determining (1) the resolution, sensitivity, and accuracy required to capture digitally the information present in the ASIP imagery and (2) the size of the computational problem involved in the required image transformations. We conclude that a properly integrated workstation involving both analog and digital video and microcomputer-based graphical components will provide a powerful and cost-effective solution to the problem posed by the ASIP data base.

PREFACE

Most of the material in this Phase I Final Report is also presented in our Phase II Proposal. Our Phase I project was designed to demonstrate the feasibility of a particular approach for the processing of the All-Sky Imaging Photometer data collected by scientists at AFGL. The results essential to that demonstration are described here. The reader interested in a full description of the target hardware and software system is referred to the Phase II proposal.

Accession For	
NTIS CRA&I	<input checked="" type="checkbox"/>
DTIC TAB	<input type="checkbox"/>
Unannounced	<input type="checkbox"/>
Justification	
By	
Distribution/	
Availability Codes	
Dist	Avail and/or Special
A-1	

TABLE OF CONTENTS

	<u>Page</u>
REPORT DOCUMENTATION PAGE	<i>i</i>
PREFACE	<i>iii</i>
TABLE OF CONTENTS	<i>iv</i>
LIST OF ILLUSTRATIONS	<i>v</i>
1. INTRODUCTION	1
2. DIGITIZATION	2
3. DIGITAL IMAGE TRANSFORMATIONS	5
4. GRAPHICS SYSTEM	8
5. CONCLUSIONS	11
FIGURES	
PLATES	

LIST OF ILLUSTRATIONS

- Figure 1. Photocopy of print made from 35-mm ASIP film image.
- Figure 2. Photocopy of print made from image recorded by airborne ASIP system.
- Figure 3. Manually prepared composite view of ASIP images from Qanaq and Longyearbyen.
- Figure 4. Film-plane to output-raster projections in a plane containing global pole, ASIP camera site, and earth's center.
- Figure 5. Video test pattern.
- Figure 6. Projections from output raster to input raster.
- Figure 7. The mapping from the digitization plane to the display window.
- Figure 8. Image-processing data flow.
- Plate 1. Sample A digitized.
- Plate 2. Sample B digitized.
- Plate 3. Test pattern digitized with vidicon TV camera using reflected light.
- Plate 4. Datacopy camera digitization at 512^2 -pixels resolution.
- Plate 5. Datacopy camera digitization at 1024^2 -pixels resolution.
- Plate 6. Sample A resampled to remove geometric distortions.
- Plate 7. Sample B resampled to remove geometric distortions.
- Plate 8. Test pattern resampled the same as sample B in Plate 7.
- Plate 9. Sample B resampled without and with anti-aliasing smoothing.
- Plate 10. Sample B resampled with assumed ASIP camera-axis tilt of 15° from vertical.
- Plate 11. Monochrome version of Plate 7.

Plate 12. "Broad-band" color scale applied to test-pattern digitization.

Plate 13. Sample B resampled and displayed with histogram equalization.

Plate 14. Synthetic composite view.

Plate 15. Example with opaque overlay in region of intersection.

Plate 16. Images are averaged locally in the region of intersection.

Plate 17. Local maximum displayed in the region of intersection.

Plate 18. Monochrome version of composite view.

1. INTRODUCTION

The ionosphere plays an important role in the operation of many communication systems and certain radar systems. A large scientific community is engaged in basic studies of the physics of the ionosphere, and much of this research is observational. The sensor systems are diverse, including orbital *in situ* sensors, satellite-beacon scintillation systems, incoherent-scatter radar, and ground-based, airborne, and orbital optical-imaging systems.

Ionospheric research at the Air Force Geophysics Laboratory (AFGL) includes a long-term auroral-observation program based on the all-sky imaging photometer (ASIP). This program currently includes three ground-based and one airborne ASIP system. Used during the northern polar night, these systems record approximately 250,000 useful images annually. These images provide an important record of the evolving, large-scale auroral activity in the polar-cap region. The image archive will continue to grow in the future, eventually totalling more than a million images. Example images are shown in Figures 1 and 2.

Currently, the ground-based ASIP images exist on reels of 35-mm film. Much of the analysis of these images is visual, with manual "cut and paste" techniques used to prepare the required formats for selected images of interest. An example is shown in Figure 3. This format is useful for interpretations because it combines the concurrent, multiple views afforded by the ASIP network. By viewing concurrent images on a map of the polar cap, perhaps with auxiliary information such as a model of the auroral oval, the analyst can begin to see the large-scale morphology of auroral patterns.

This presentation is misleading, however, because each image retains the wide-angle lens distortions inherent to photographic observations of this type. This distortion is shown schematically in Figure 4. As a consequence, positions are correct in the composite format (Figure 3) only at the center of each field of view (FOV). Features near the edge of each FOV are severely distorted, essentially by a compression in the radial direction.

These manually prepared composite views are also awkward to produce.

Clearly, it would be impossible to convert any but a small fraction of the available images to this format.

For the purposes of interpretation and presentation, it would be useful to show composite ASIP views with a variety of correlative data from other sensors, such as incoherent-scatter radar and the sensors on board the HILAT satellite. These independent measurements would provide useful coverage co-located and concurrent with the ASIP observations. (The relevant HILAT data are summarized in the table on the following page.)

It thus seems clear that an image-processing system is needed that will (1) deal with the volume of the ASIP images, providing convenient access to the entire archive of on the order of 10^6 images, (2) remove the projective distortions and generate an accurate large-scale map of the observed auroral activity, and (3) provide convenient graphics and computational tools for assembling displays that combine the multiple ASIP imagery with a variety of correlative data, as required for the purposes of interpretation and presentation.

In our Phase I SBIR study, we demonstrated the feasibility of satisfying the above needs. The approach taken involved a combination of video imaging and recording, digital image processing, and computer-aided raster graphics. In order to prove that this approach is appropriate, we addressed the following specific questions: (1) What resolution and sensitivity is required in the digitization of the ASIP images? (2) Is the video-disc medium appropriate to store the ASIP archive? (3) Can the geometric correction processing be performed interactively on a microcomputer system? (4) Are the digitally processed and enhanced ASIP images successful in revealing information not readily accessible in the raw images?

2. DIGITIZATION

For the purposes of determining digitization resolution and sensitivity requirements, and to test the geometrical transformation processing, we concentrated on a few test images. These are shown in Figures 1, 2, and 5, which are, respectively, sample ground-based and airborne system images, and a video test pattern.

Table: HILAT data relevant to All-Sky interpretations. Certain HILAT observables are omitted either because they are not operational or not directly accessible. Non *in situ* measurements sample along various lines of sight, either to an external receiver or nadir directed. The geometries of these sample paths will need to be accounted for to show these data in correct relationship with the All-Sky images.

Payload	Observables	Sample Altitude	Sample Path	Dimensionality
Beacon	σ_ϕ, S_4^*	F layer	xmtr-rcvr	scalar
	COR*†	F layer	xmtr-rcvr	vector (2)
	TEC	F layer	xmtr-rcvr	scalar
Plasma Monitor	N_i	800 km	<i>in situ</i>	scalar
	\vec{V}_i	800 km	<i>in situ</i>	vector (2)
Magnetometer	$\vec{\Delta B}$	800 km	<i>in situ</i>	vector (2 or 3)
Electron Spectrometer	JTOT	800 km	<i>in situ</i>	scalar
	JETOT	800 km	<i>in situ</i>	scalar
	EAVE	800 km	<i>in situ</i>	scalar
	Spectrum	800 km	<i>in situ</i>	array (8 or 16)
AIM Photometers	6300 Å	F layer	nadir	scalar
	3914 Å	E layer	nadir	scalar

* These quantities also available from beacons on other satellites.

† Axial ratio and orientation of correlation ellipse.

Sample digitizations were obtained using two cameras. The first camera was an RCA closed-circuit TV camera, Model TC-2511. This is a 2/3" vidicon-tube camera rated at better than 600-lines resolution. It produces an EIA RS-170 standard monochrome video signal. This signal was digitized with an Imaging Technology PC-Visions 6-bit video digitization board in a Compaq microcomputer. This particular digitization board captures 512^2 , 6-bit pixels in one video frame time, 1/30th second. Several test images were recorded with this set up. Three (corresponding to Figures 1, 2, and 5, respectively) are shown in Plates 1, 2, and 3. Sample A (Plate 1) was taken directly off one of the ASIP 35-mm film frames with back lighting. Sample B (Plate 2) and the test-pattern digitization (Plate 3) were taken off full-size prints with reflected light.

The plates presented here are 35-mm photographs of our RGB monitor screen. The screen raster measures 512 x 480 pixels. Any single display can have up to 256 distinct colors, selectable from a palette of over 16 million colors. Various false color scales are used here to represent intensity.

Comparing Plates 1, 2, and 3 with Figures 1, 2, and 5, respectively, we see that the fidelity of the digitized images is generally high. In Plate 2, the stars and antenna wires are clearly visible. The test pattern (Plate 3) is reproduced with acceptable levels of resolution and geometrical accuracy.

The second digitization approach used the Datacopy Model 610 Digitizing Camera. Unlike the vidicon camera described above, the Datacopy camera does not produce an RS-170 signal (and hence does not produce a picture directly viewable on a TV monitor). It is a scanning system, based on a linear CCD array. It is capable of providing variable resolutions up to 1728 x 2846 pixels, with 8-bit sensitivity. For our tests, we obtained both 512^2 and 1024^2 digitizations of sample B (Figure 2). The results are shown in Plates 4 and 5. A comparison of these two plates indicates that the original image contains little useful information in scales smaller than about 1/500th of its width.

We concluded that high-definition, monochrome video resolution (EIA RS-170) is appropriate for the ASIP imagery. This is an important result because it opens the door to a system combining relatively economical video recording

and digitization technology. We evaluated video-disc media and identified a particular device, the Panasonic OMDR, that offers high storage volume (nominally 15,000 images per disc), good resolution (450 lines minimum), and fast, random access to any image. This device is unique because it offers both reading and writing (write once, not erasable) in a single unit. All other video disc media require premastering and are suitable only for mass reproduction applications. An ASIP file-management and processing workstation based on this device for image storage is described in our Phase II proposal.

3. DIGITAL IMAGE TRANSFORMATIONS

The major focus of our work in Phase I has been the transformation from ASIP camera view to composite, global view. Most of the transformation problem is concerned with projective geometry. A mapping exists that relates the input raster, defined in the digitization setup, to the output raster, which will usually represent the image displayed on an RGB monitor. Our job was to derive that mapping and devise an efficient algorithm for its implementation. There are also some second-order distortions that can be corrected in this stage of the processing. These have to do with certain radiometric effects associated with the ASIP imaging system and with possible video distortions originating with the film-to-video translation step. Our goal was to be able to carry out the geometrical correction processing for a given image fast enough to be consistent with interactive, as opposed to batch, processors.

The projective transformations may be understood by considering the sequence of mappings involved in going from a point in the output raster to the position of that same point in the input raster. The situation is shown schematically in Figure 6. In this discussion we will adopt a raster coordinate system (X,Y) such that integer values correspond to the pixel centers, with $(0,0)$ in the lower-left hand corner. Pixel intensity will be denoted by Z , which, for an 8-bit device, will adopt integer values in the range $(0,255)$. Hence, the intensity of a particular pixel in the output raster (OR) may be denoted $Z_{OR} = Z(X_{OR}, Y_{OR})$. The output plane generally will represent a polar

projection of some particular ionospheric layer. Thus, there exists a mapping from (X_{OR}, Y_{OR}) to $(\phi_{ISG}, \theta_{ISG})$ where ϕ and θ denote spherical coordinates measured on the ionosphere with respect to a global pole (ISG). (We could also use latitude and longitude here, but for notational consistency with other spherical systems to follow, we adopt the more general spherical coordinate notation.) The global pole will usually be the magnetic north pole, but any position, for example the geodetic pole, also could be used. Next, using the principles of spherical geometry, we can transform to $(\phi_{ISZ}, \theta_{ISZ})$, which are the spherical angles measured on the ionosphere with respect to the zenith at an ASIP camera site. The ASIP camera sees the ionosphere as if projected onto a spherical surface centered at the camera. Thus, we next transform to $(\phi_{ASZ}, \theta_{ASZ})$, which are the spherical angles on the ASIP-centered sphere measured relative to the local zenith. In general, the ASIP camera axis will not correspond exactly to the zenith direction, due to small alignment errors. Another spherical transformation is required to get to $(\phi_{ASC}, \theta_{ASC})$, the spherical coordinates measured on the ASIP sphere with respect to the camera axis. Next, we have the ASIP lens projection which takes us to (X_{FP}, Y_{FP}) , which are the cartesian coordinates measured on the film plane (FP). Finally, we have the film-to-video and digitizer projections, which take us to (X_{IR}, Y_{IR}) on the input raster (IR). In general, of course, X_{IR} and Y_{IR} will not be integers, which means that the image of an output pixel on the input raster does not fall on top of one of the input pixels. An interpolation is required to determine Z_{OR} from Z_{IR} , the input raster data. A variety of interpolation schemes is applicable, for example: nearest neighbor, best-fit polynomial, bicubic splines, and others. We find that bilinear interpolation works very well here because of the rectangular geometry of the sample points. Thus, letting I and J be the integer parts of X_{IR} and Y_{IR} , we have:

$$\begin{aligned}
 Z(X_{OR}, Y_{OR}) = & Z(I, J) + (X_{IR} - I) [Z(I + 1, J) - Z(I, J)] \\
 & + (Y_{IR} - J) [Z(I, J + 1) - Z(I, J)] \\
 & + (X_{IR} - I) (Y_{IR} - J) [Z(I, J) + Z(I + 1, J + 1) \\
 & \quad - Z(I + 1, J) - Z(I, J + 1)] .
 \end{aligned}$$

The parameters involved in the above transformations include the following: the size of the output raster (number of pixels per scan and numbers of scans); the height and width of the output window; the position of the global pole in the output window; the orientation of the output window with respect to the global system; the radius of the earth and the assumed height of the emission region; the latitude and longitude of the global pole (usually taken to be the north magnetic pole); the latitude and longitude of the camera site; azimuth and elevation of the camera axis relative to the local zenith; the camera field of view in terms of an elevation angle measured relative to the camera axis; the height, width, and orientation of the input raster; the position of the center of the ASIP FOV in the input raster; and the size of the input raster.

Figure 7, which is from the Phase I proposal, is a schematic showing the relationship between the input and output rasters. We see that, owing to the viewing geometry inherent with the ASIP system, the input resolution is greatest near the zenith, or image center. Hence, to avoid aliasing errors, the image data should be smoothed in the input raster domain prior to resampling to the output raster. Essentially, we want each output pixel to represent the average of all those input pixels mapped onto the cellular domain of that output pixel. Obviously, the required smoothing is two-dimensional and variable; in the example shown in Figure 7, no smoothing at all is required near the edges of the frame, and up to four-point smoothing in both x and y is required near the center. An example is presented below demonstrating the effect of this type of smoothing.

The transformation processing is depicted in Figure 8. Fundamental to our approach is the separation of the transformation-dependent processing from the frame-dependent processing. For a given output format, which involves the specification of the output window size and position, all the computations involved in the mapping between the input and output rasters can be carried out and the results saved. These results are in the form of three schedule, or control, files which are used each time a particular frame is processed. This makes the frame-dependent processing very efficient, mostly

involving integer arithmetic and only a minimum of floating-point operations. The schedule files govern the x and y smoothing and the resampling. The generation of the schedule files requires many floating-point operations because of the trigonometry involved in the transformations. Fortunately, these files need to be generated only when a new display format is required, not each time an image is processed. Schedule file generation takes approximately one hour on the IBM PC/AT and, therefore, should not be part of an interactive session.

Examples of the transformation processing appear in plates 6, 7 and 8 which show the transformed and resampled versions of the samples shown in Figures 1, 2, and 5, respectively. We see that the most striking effect of the transformation (aside from the inversion from upward view to downward map projection for the ASIP images) is to stretch radially features near the limb, and compress features near the center. This also produces an apparent defocusing near the limb, relative to the center. These effects are most apparent in Plate 8. In Plate 7 we see that the antenna wires have been straightened, which is, of course, what we expect since the wire curvature in the raw image was introduced by the "fish-eye" lens distortion.

As discussed above, the transformation processing includes a smoothing step necessary to prevent aliasing errors in the central region of the image where the output raster generally undersamples the image data. A demonstration of the effect of this smoothing is shown in Plate 9.

A demonstration of the effect of ASIP camera-axis tilt is presented in Plate 10. The data are from Figure 2 again, and this result should be compared with Plate 7. A fictitious, 15° camera-axis tilt was assumed. In this case, the FOV will extend much farther on the ionosphere in the direction of tilt, and this produces the elongated image seen in Plate 10. This is an exaggerated example, as the ground-based ASIP cameras are generally aligned with the vertical to within 2° .

4. GRAPHICS SYSTEM

As part of our Phase I effort, we have developed a hardware and software system which provides many of the graphics capabilities which would be

required in a production system. The hardware includes the following: IBM PC-AT computer, Number Nine graphics adapter, and Electrohome analog RGB monitor. The software includes interactive graphics routines for the display of both pixel, or image, data and vector data. A number of output formats were developed, including composite displays with multiple ASIP images, coastlines, coordinate lines, and HILAT data.

We found the continuous-color capabilities of the analog RGB display to be highly desirable. As an example, a monochrome version of Plate 7 is shown in Plate 11. Although the latter is, perhaps, more realistic, the color version reveals more of the structural details, such as the stars and certain portions of the wires. This is not surprising, of course; it is well known that the human eye can distinguish many more colors than shades of gray. Thus, false colors definitely are useful in this application, and the analog RGB display is needed to represent adequately these colors. We will also see below how the color capabilities of this type of display are useful in the presentation of multivariate data.

The frame-buffer architecture employed in this system is very powerful for implementing image-enhancement approaches based on color-scale manipulations. This is because the colors viewed on the screen can be changed simply by changing the color look-up table. This can be done essentially instantaneously, as opposed to the several seconds required to modify the contents of the frame buffer.

An example of the effects achievable by color-table changes is shown in Plate 12. These are the same data as in Plate 3, but with a new color table. The color scheme is very unnatural in appearance, and it does not improve the readability of the image, but it does enhance the subtle variations in lighting that exist across the image.

Another example is shown in Plate 13. Here, the color table has been transformed based on the image histogram. The effect is to produce an image with an approximately equalized histogram--there is an equal amount of each color, roughly speaking. (Discrete sampling effects prevent the realization of perfect equalization.) Although for this particular image the effect is

not particularly desirable, the example does serve to demonstrate the power of color-table manipulations in modifying the visual impact of the display. Obviously, it must be left to the individual user *whether or not* any of these enhancement techniques should be used in a particular case.

An example composite view is shown in Plate 14. This is a synthetic view, made up here for the purposes of demonstration. All data are real, including the HILAT data, but are not concurrent (time and date information shown in the legend is fictitious). This is a representative format that might be used for interactive, interpretive purposes, or, in hardcopy, for publication. Any number of ASIP images could be combined in this way, including one from the airborne system. The HILAT data are presented on a spatially correct abscissa so that associations with the image data will be approximately valid. (Time and altitude discrepancies are still present.) This example also demonstrates how colors can be used to clarify the data relationships in a complex display involving several variables.

The geographically astute reader may notice that the ASIP site placements in this view are not quite correct. An inconsistency (approximately 2° in longitude) between the magnetic coordinate systems used for the coastline data and the image data existed in our codes when this view was assembled. This will be corrected in future processing.

We see in Plate 14 that for 300-km auroral emissions, the ASIP fields of view from Qanaq and Sondrestromfjord overlap by more than 30%. A decision has to be made when assembling the composite view as to how to handle the overlap region. Three possible approaches--opaque overlay, local average, and local maximum--are demonstrated in Plates 15, 16, and 17. Again, the user will need to choose the method best suited for his particular case. Probably the opaque overlay is the most reliable of the three techniques demonstrated here. For interactive viewing, the user can easily reverse the sequencing of the overlaid images and will thus not really be prevented from seeing all of both images.

A monochrome version of the composite display is shown in Plate 18. We see that although there is some loss of visible information, particularly

within the ASIP FOVs, the monochrome display is generally successful here. In fact, the annotations are slightly more legible in black and white. Generally speaking, we expect that the color display formats will be preferred for interactive viewing, and the monochrome displays will be selected when hardcopies are needed for publication.

5. CONCLUSIONS

We find that the ASIP images can be faithfully represented with RS-170 video resolution. We therefore have a wide selection of video hardware to choose from in Phase II. It will be important for this application to choose a high-definition TV camera with low geometric distortion. In video form, the images will be recordable on the Panasonic OMDR. The high-definition, monochrome version of this device is the appropriate choice. We established that the video images, which could originate either from a TV camera or from a video recording device, can be conveniently digitized using any of a variety of IBM PC bus-compatible digitizer boards. A more detailed discussion of the video hardware options is given in the Phase II proposal.

The digital processing to correct for geometrical distortions was developed and tested on our IBM PC/AT system. By appropriately organizing the computational steps, we find that the image-dependent processing can be carried out in approximately one or two minutes, depending on the size of the image. We expect to make this processing faster in Phase II. The important point here is that the processing can be done interactively on a micro-computer-based system.

Finally, we developed an interactive graphics system, also based on the IBM PC/AT. Composite formats involving the geometrically correct ASIP images, HILAT data, coordinates, and annotations were produced with this system. These formats, and others that the users would be free to invent, should be very useful in the interpretation of the data.

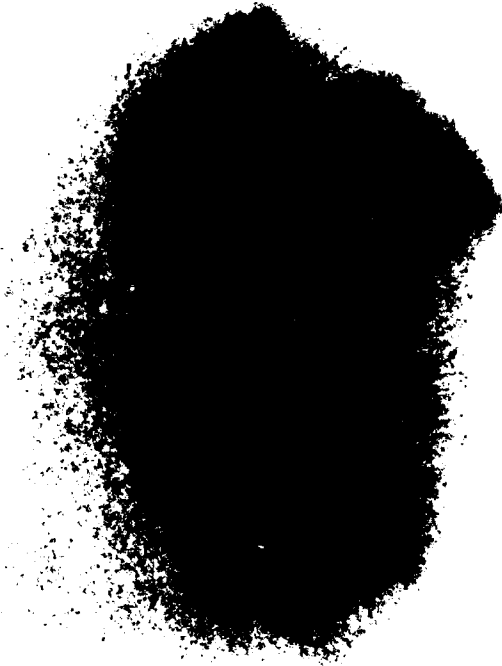


Figure 1. Photocopy of print made from 35-mm ASIP film image. Frames are recorded in half-frame format. Number indicates date, time, and filter number. Exposures alternate between two filters, 4278 and 6300 Å.

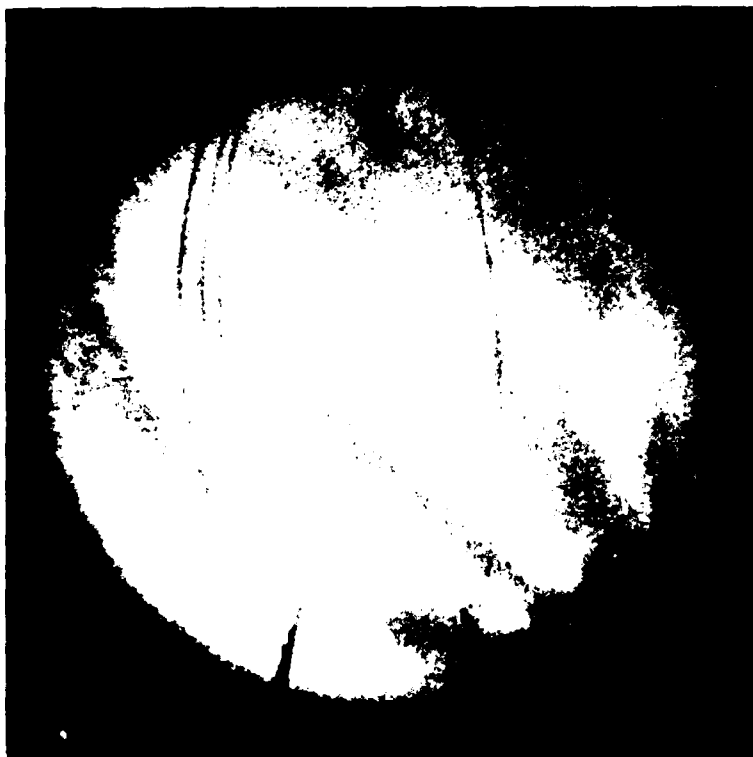


Figure 2. Photocopy of print made from image recorded by airborne ASIP system. This image was used for test purposes because it contains unusually detailed features that challenge digitization resolution and processing accuracy. Aircraft antenna wires are visible. Stars are also visible in original print.

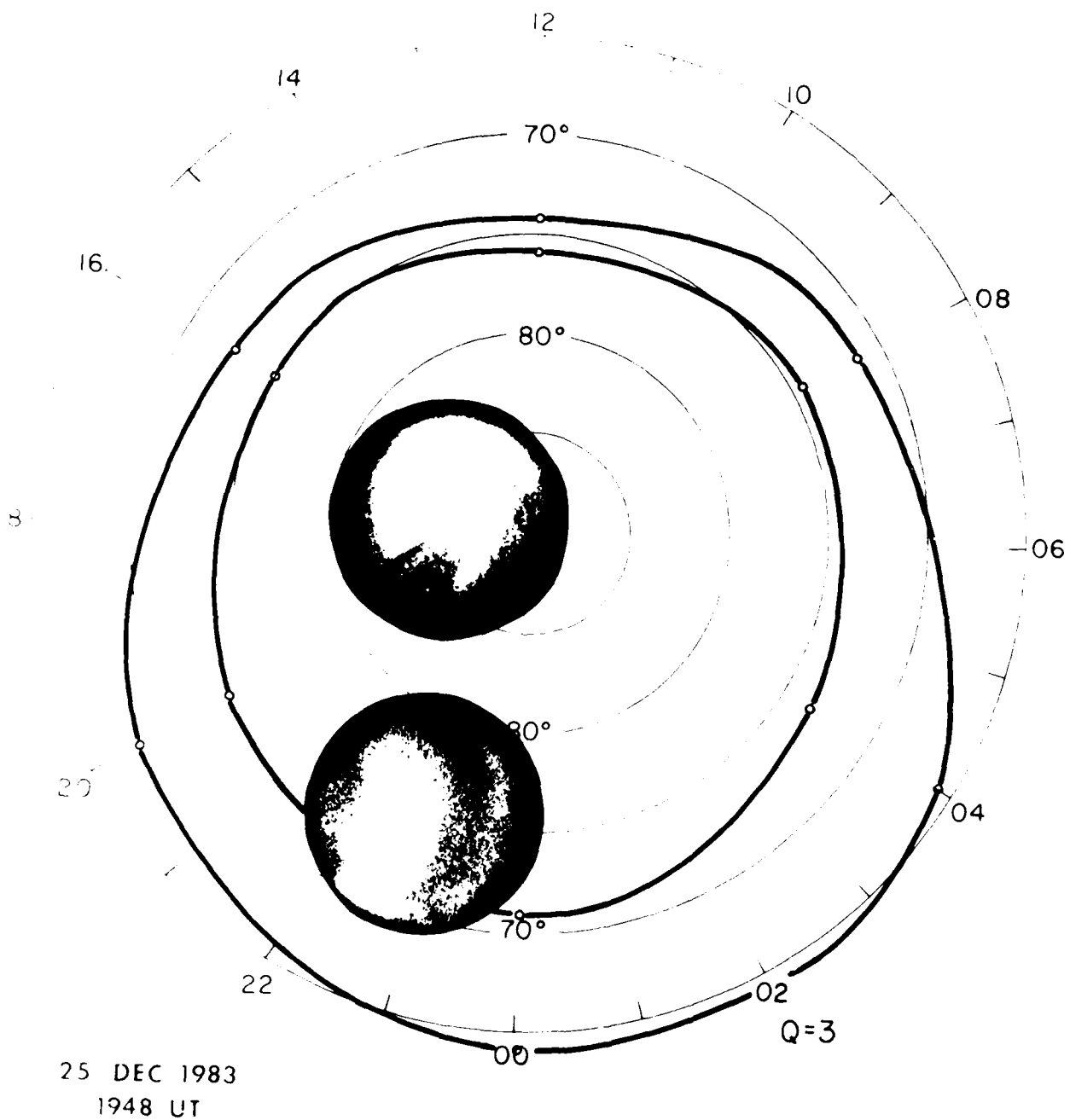


Figure 3. Manually prepared composite view of ASIP images from Qanaq and Longyearbyen. (Photocopy of photographic print obtained from AFGL.) Cutouts from photo enlargements are here overlaid on magnetic coordinate system. The auroral oval is also drawn. In this type of display, only the centers of the two images are positioned correctly. Wide-angle lens distortion introduces appreciable foreshortening near the edges of the FOVs.

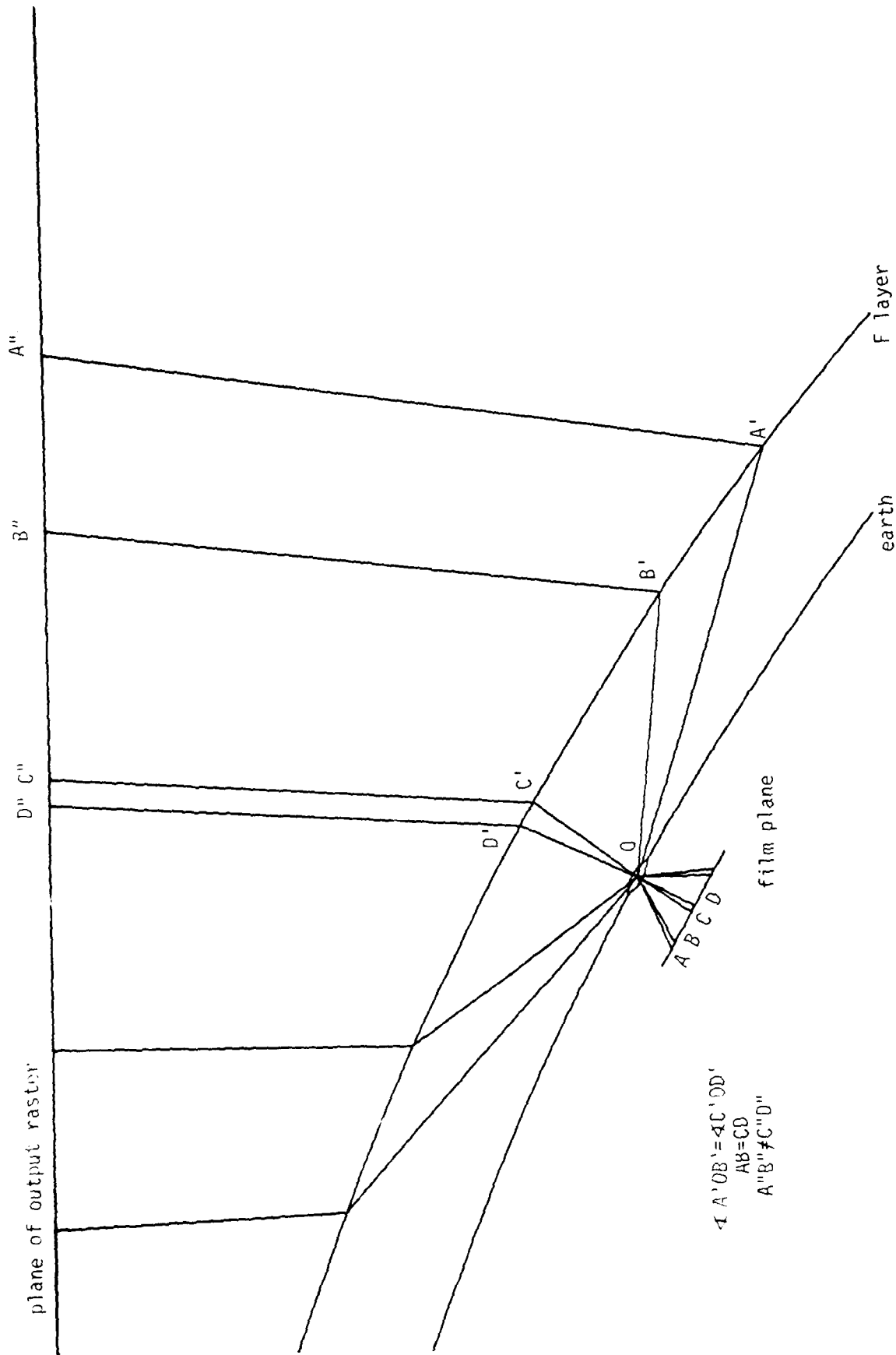


Figure 4. Film-plane to output-raster projections in a plane containing global pole, ASIP camera site, and earth's center. Nominal F layer at 300 km has been assumed. Height of F layer is drawn to scale relative to the earth's curvature and the ASIP field of view. The projection from the output raster to the ionosphere preserves equal latitude increments. The projection from the ionosphere to the film plane preserves equal increments of the elevation angle with respect to the local horizon. Note that features near the edge of the field of view will appear on the film nearly five times smaller than similar features overhead.

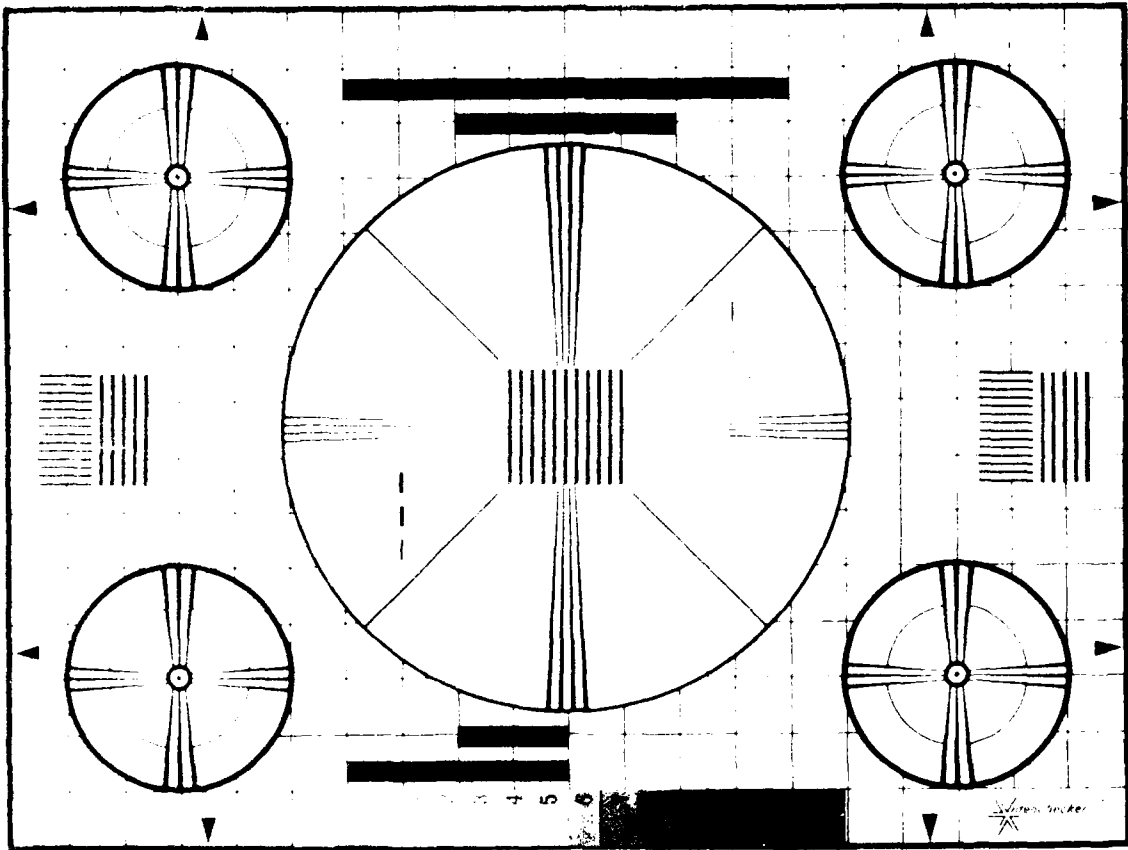


Figure 5. Video test pattern.

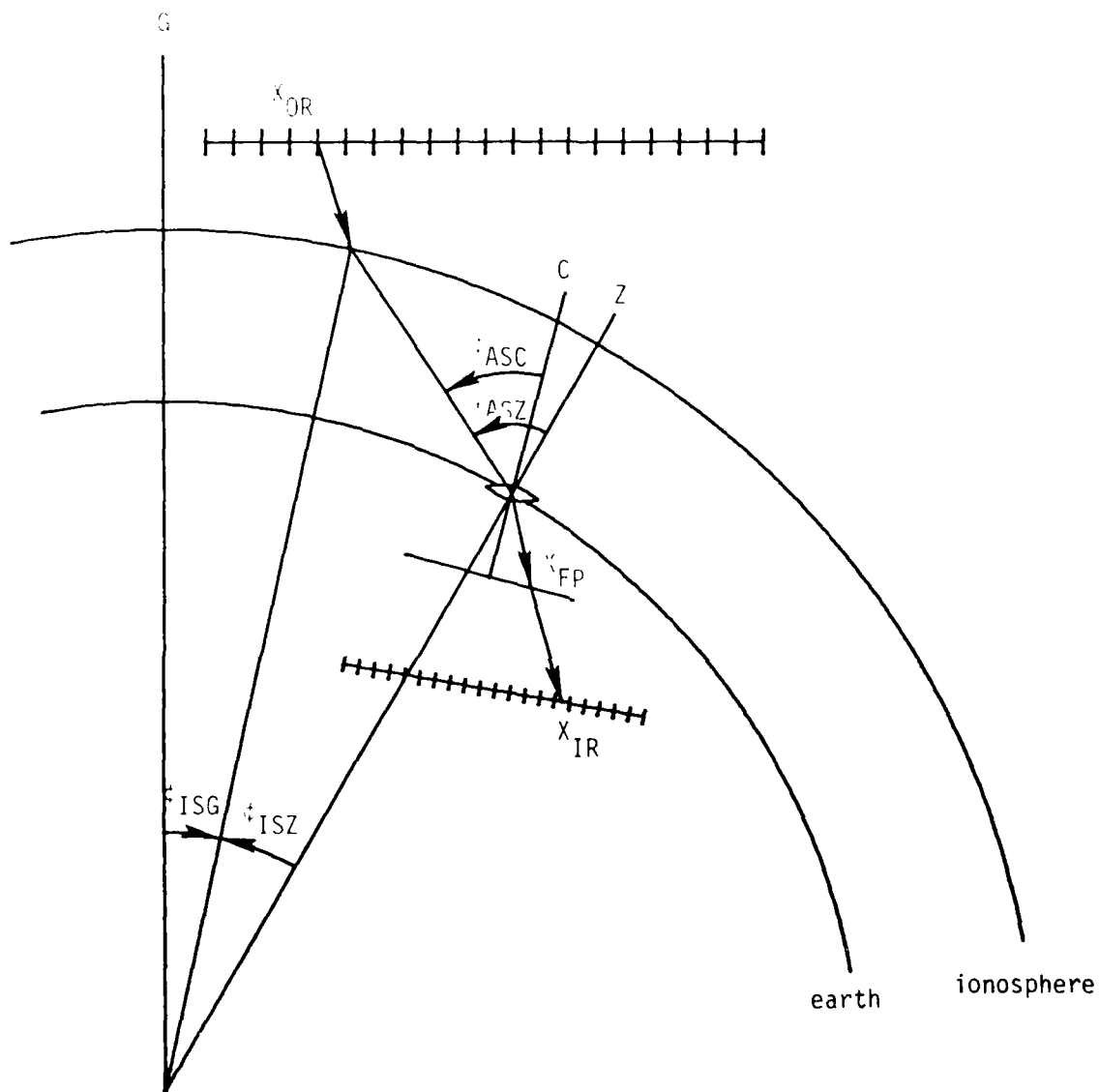
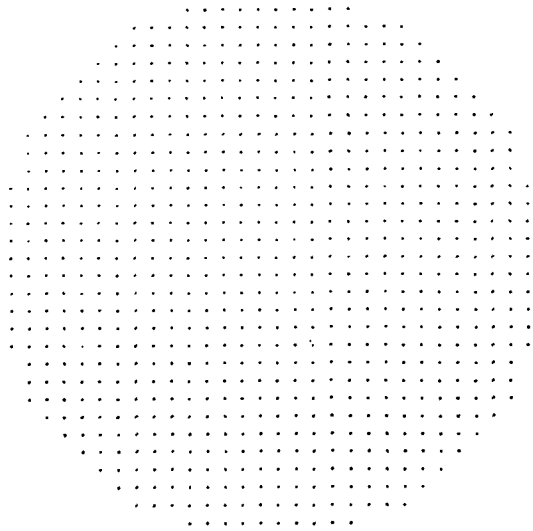
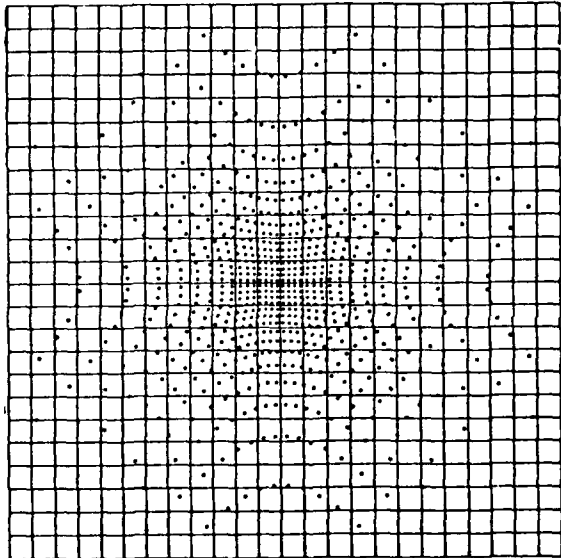


Figure 6. Projections from output raster (OR) to input raster (IR) (not to scale). G indicates global pole, C and Z are ASIP camera axis and local zenith, respectively. Ticks on OR and IR indicate raster-element positions. Note that the image of an output pixel on the input raster will generally not coincide with an input pixel. The intensity displayed at X_{OR} must be determined by interpolating on the input raster plane.

All-Sky frame digitization array



Digitization points transformed to display window



Decimated digitization points in display window

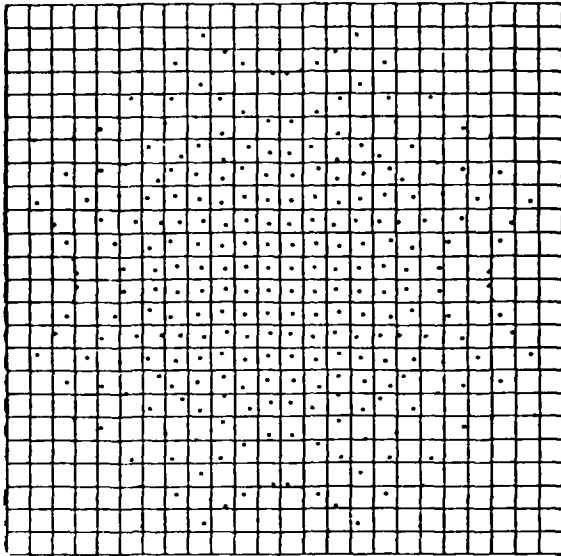


Figure 7.

The circular region of dots on the left depicts a 32x32 digitization of an ASIP image frame. Note that the digitization positions form a rectangular array. (Positions outside of the 155-degree FOV are not shown here.) After digitization the image exists as a matrix of numbers representing the optical density at each of these positions. To construct a top view, or map, of the auroral phenomena recorded by the camera, we must project the digitized data back to their points of origin, which we typically take to be on either the F or E layers. The effect of this transformation is shown in the center panel. Here we see the same set of points mapped onto a display window representing the map view. We see that the mapping deforms the digitization array so that it is no longer rectangular.

The grid of lines in this figure represents a 24x24 array of display picture elements. The image will be created by adjusting the intensity of each cell within this grid. (In actual practice, the digitization and display resolutions will be much higher than we use here for expository purposes.) We see that near the center of the image each pixel corresponds to several of the original samples, whereas near the edges the samples are sparse, and there are few or no samples per pixel. Therefore, the pixel intensities are determined by an averaging operation near the center and an interpolation near the edges. If we locally average the samples so that we have only one (or less) data point per pixel, we obtain the arrangement shown on the right. Here the position of each dot is the average position of all samples falling in the respective cell, and the data value associated with that dot is the average of those data values. Pixel intensities are now computed from these data by 2D interpolations.

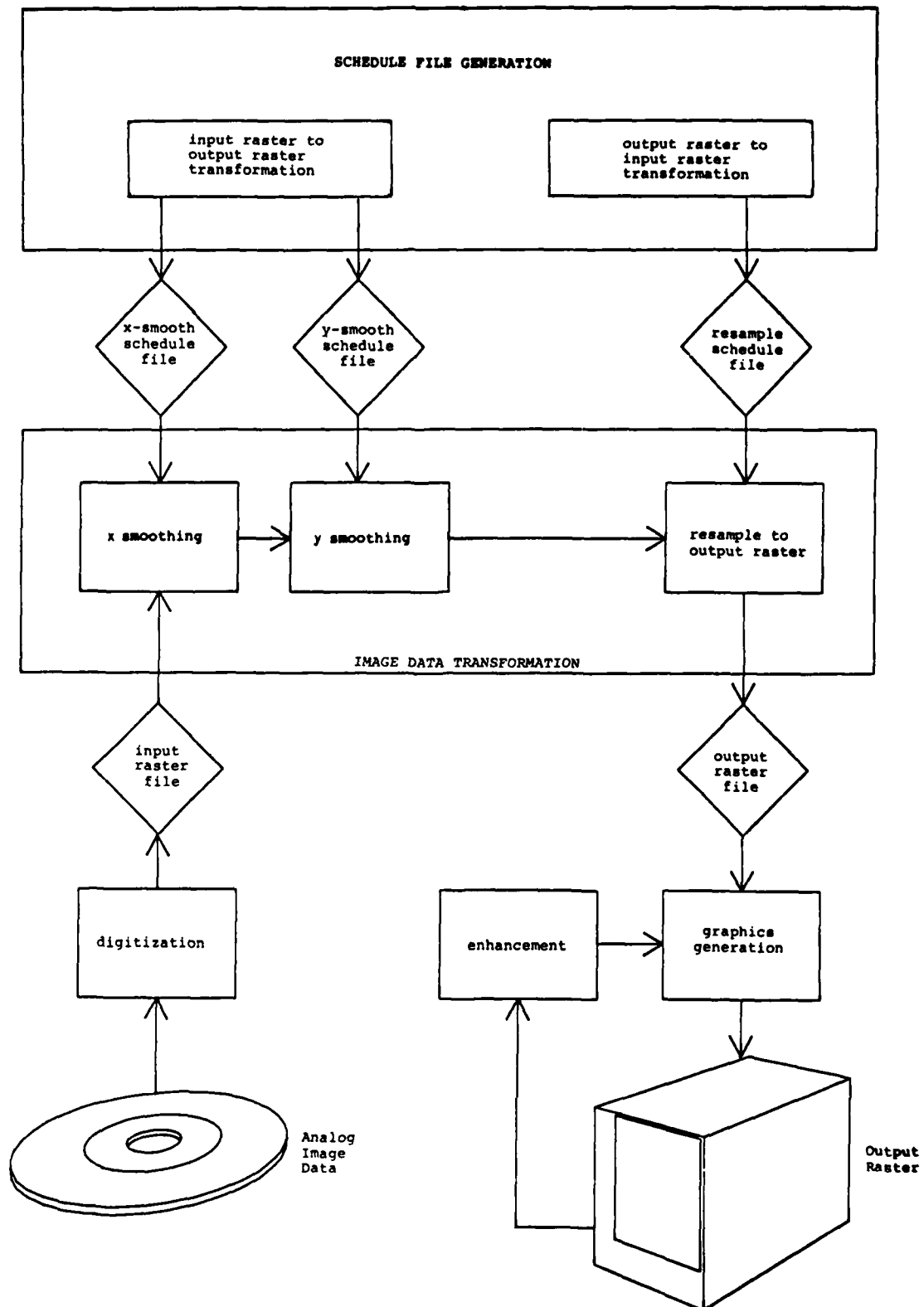


Figure 8.

Image-processing data flow. Raw image is in analog form on video disc. Images of interest can be accessed randomly, digitized, transformed to the output raster, and viewed interactively on the monitor. Processing time for one image will be approximately one minute. Processing is controlled by schedule files which are pre-computed for a given output format (size and position of output window in world coordinates). Schedule file generation will take on the order of one hour for each output format. (Estimated times are for IBM PC/AT.)

RASTER SCREEN DISPLAYS (PLATES)

The following plates are 35-mm SLR photographs of the RGB monitor screen using Kodacolor 200 film. A one-half second exposure was used. To the eye, the live screen is brighter and more pleasing than the prints. While shooting directly off the screen in this way will yield acceptable hardcopies, a better approach, the one proposed for the Phase II workstation, is to use a film-copier device (many are commercially available) specifically designed to produce quality film copies of raster displays.



Plate 1. Sample A (see Figure 1) digitized. Data captured by vidicon TV camera directly off 35 mm ASIP film with backlighting. Colors are false, with red indicating white and blue indicating black



Plate 2. Sample B (see Figure 2) digitized. Data captured by vidicon TV camera directly off print with reflected light. Print is airborne ASIP system image. Bright red points are stars. Four antenna wires are visible. Their curvature is produced by wide-angle lens distortion. Yellow margin is paper mask overlayed on the image when TV picture was taken. Color variations around mask are due to nonuniformity of illumination

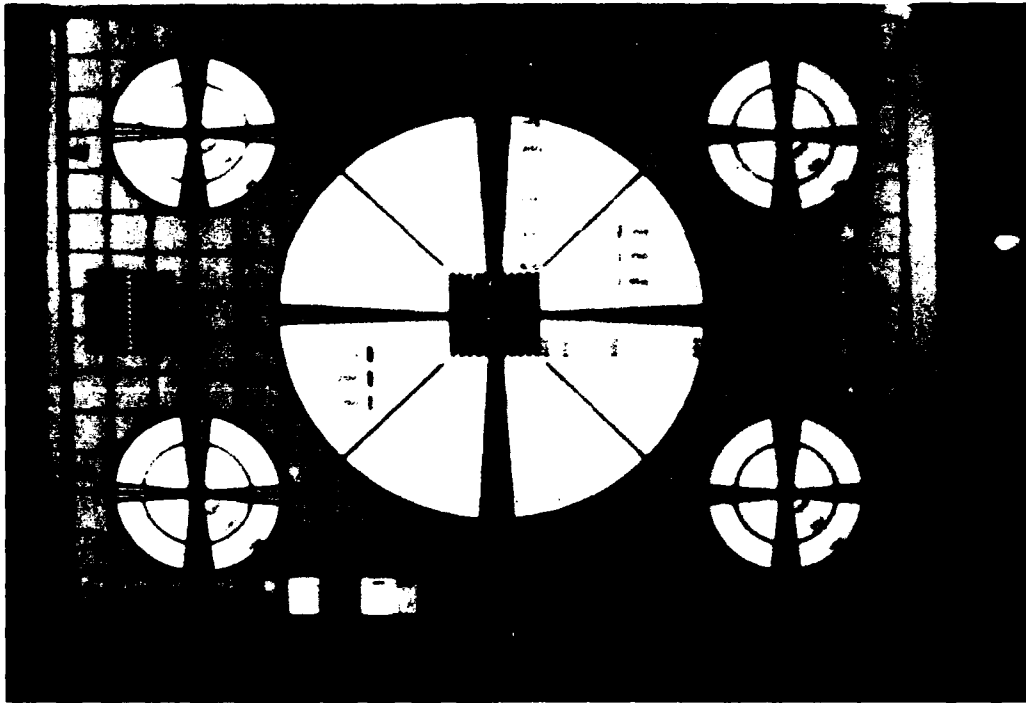


Plate 3. Test pattern digitized with vidicon TV camera using reflected light. Note that illumination is not uniform. Areal imaging to be used in Phase II system should result in very even illumination, center to edge



Plate 4. Databook camera digitization at 512^2 pixels resolution. Image in this view has been enlarged (zoomed with pixel replication) by a factor of 2. Thus, only a 256×240 subset of the full data array for this image is seen here. Compare this image with vidicon camera view seen in Plate 2



Plate 5. Databook camera digitization at 1024^2 pixels resolution. Window shows only a 512×480 subset of full data array. Compare this image with Plate 4. Note that the higher resolution digitization picks up very little additional detail. Hence, original image contains practically no information in scales smaller than $1/500$ th of the image dimension



Plate 6. Sample A (Plate 1) resampled to remove geometric distortions. Note that data are clipped at the edge of the ASIP FOV (155°)
Effect of transformation is to stretch radially features near limb, relative to center

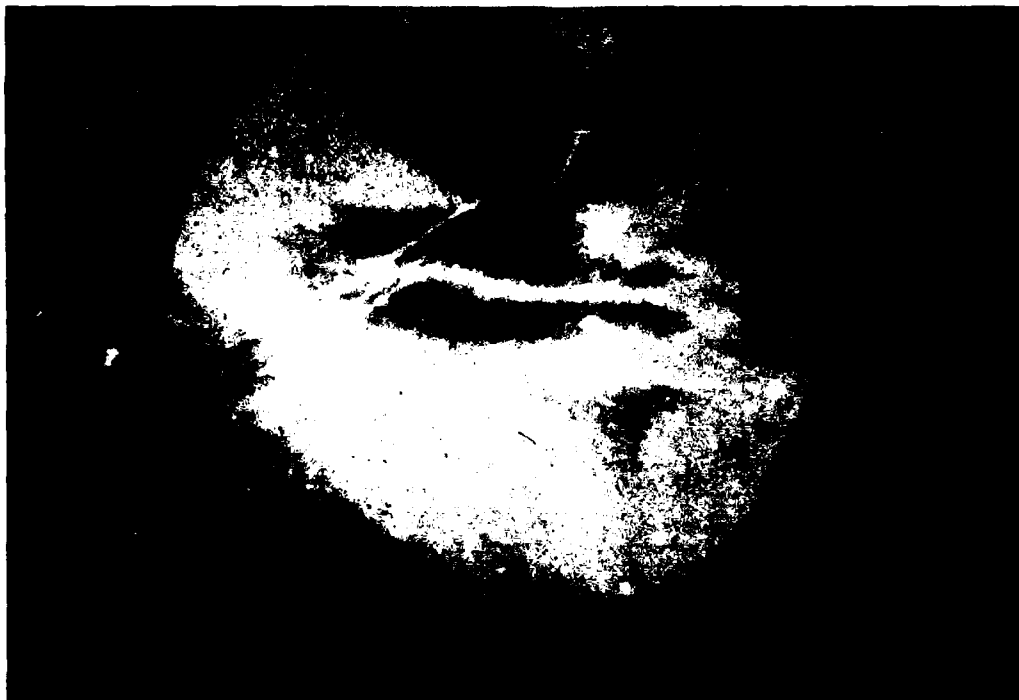


Plate 7. Sample B (Plate 2) resampled to remove geometric distortion. Note that the antenna wires are now straight. Stars in central region are still visible, but stretching near limb appears to defocus the image there



Plate 8. Test pattern (Plate 3) resampled the same as sample B in Plate 7. Geometrical effect of transformation is apparent, including apparent defocusing away from central region



Plate 9. Sample B resampled without (left half) and with (right half) anti-aliasing smoothing. To make the effect more apparent, output resolution was reduced by a factor of 4 (128 x 120) relative to Plate 7. A fourfold zoom has been applied to bring the image back to full size for ease of comparison. Note that the effect of smoothing is most visible near the center where the input raster is dense relative to the output raster. The undersampling in this region will produce slight aliasing effects when the smoothing step is omitted



Plate 10. Sample B resampled with assumed ASIP camera axis tilt of 15° from the vertical. The FOV projected onto the ionosphere is no longer circular. (Compare with Plate 7) The misalignment assumed here for purposes of demonstration is exaggerated; actual ASIP camera installations (groundbased) are aligned very close to the zenith, typically within 2°



Plate 11. Monochrome version of Plate 7. Color photos generally produce a greater dynamic range than monochrome, as is the case here. Visual comparisons of the color and monochrome images on the CRT give a similar impression with additional detail generally visible in the color versions.



Plate 12. "Broad-band" color scale applied to test-pattern digitization. (Compare with Plate 3). Color scale is overlaid across top of screen. This scale is useless for indicating relative highs and lows, but it does a very good job of revealing small variations. In this case, the illumination nonuniformities become very conspicuous.



Plate 13. Sample B resampled and displayed with histogram equalization. (Compare with Plate 7.) This enhancement technique attempts to locate the color scale equally, according to the histogram of intensity values in a selected subset of the image. Color-scale (or gray-scale) image enhancement approaches like this one are very efficient on frame-buffer displays and can easily be viewed interactively.

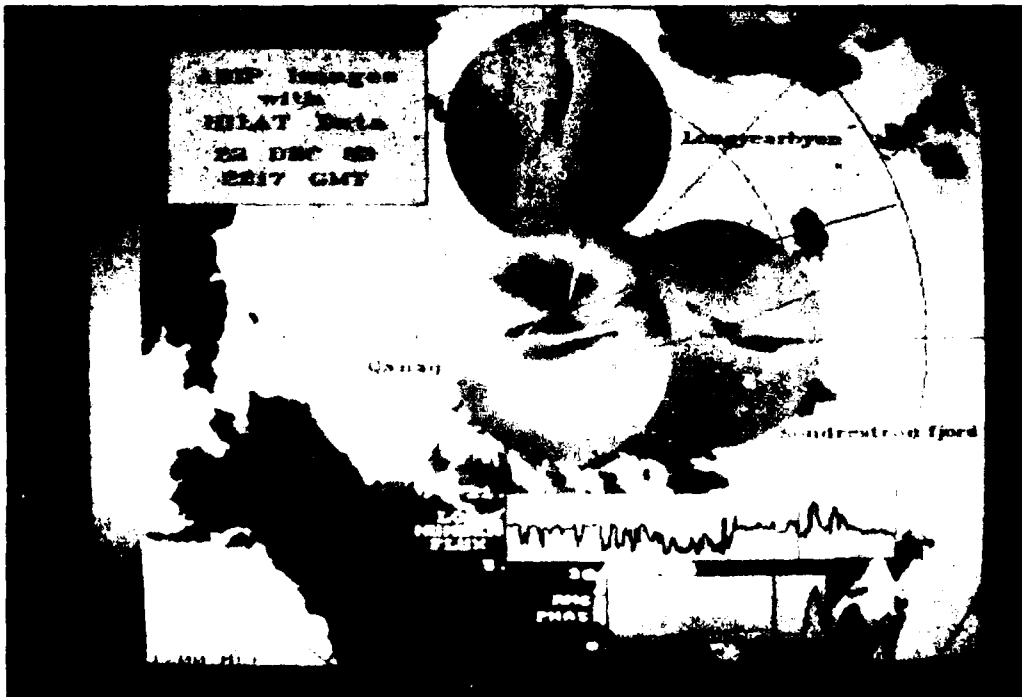


Plate 14. Synthetic composite view. All data are real, but not actually concurrent. Hence, any correlations among the different ASIP images or with the HILAT data are strictly coincidental. Assumed altitude of the emission layer is 300 km. Satellite trajectory is shown in red and the transmitter-receiver penetration point for Sondrestromfjord is shown in blue. Hence, the plasma number flux data are *in situ* at 800 km while the scintillation data are roughly co-located with the aurora. HILAT data are time series, and the time of ASIP image collection is indicated here by a vertical line across plot windows. Format here is only an example. In actual practice, these displays would be generated interactively in formats suiting special purposes of the user.



Plate 15. ASIP fields of view may overlap in composite view. User will have to decide how to handle the intersection. If the opaque overlap option is used, as shown here, part of one of the images will be lost from view. Other options are demonstrated in Plates 16 and 17.



Plate 16. Images are averaged locally in the region of intersection. Information from both images is visible, but effect may be confusing.



Figure 17. The same two images as in the region of intersection. Images blend together here (compare with Plates 15 and 16), but again, the two patterns are presented separately. The local average or local maximum presentation should be used only when the two images overlap in the region of overlap.

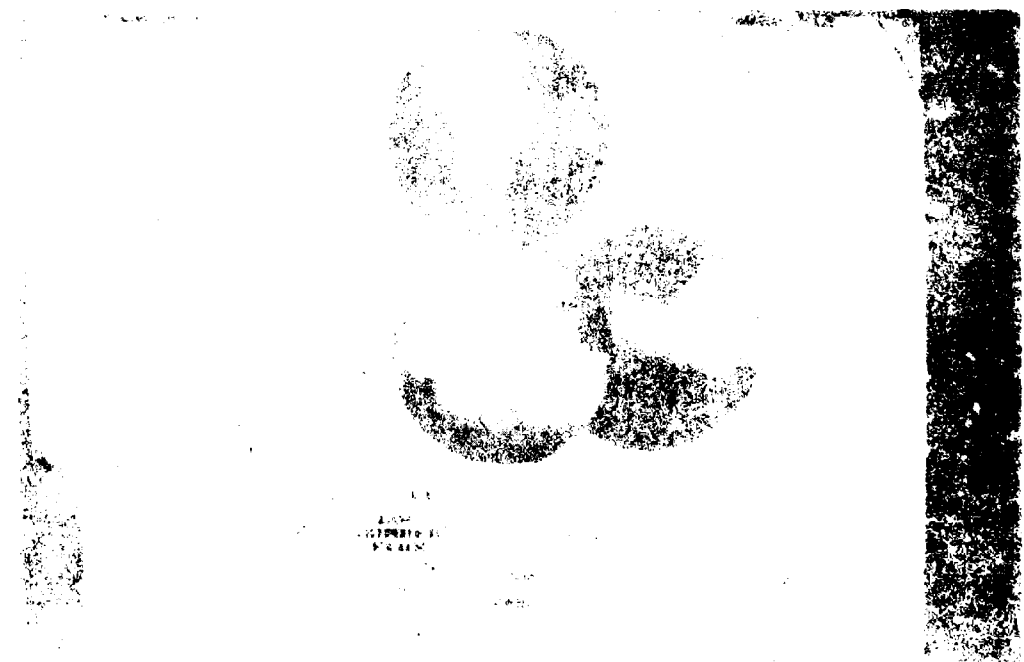


Figure 18. The same two images as in the region of intersection, compare with Plate 14. With this presentation, which is usually by slight variation to components, the two images are presented separately. The local average or local maximum presentation should be used only when the two images overlap in the region of overlap.

END

FILMED

386

DTIC